Membrane potential and spike train statistics depend distinctly on input statistics

Robert Rosenbaum[1] and Krešimir Josić[1,2]

[1]*Department of Mathematics, University of Houston, Houston Texas 77204-3008, USA*
[2]*Department of Biology and Biochemistry, University of Houston, Houston Texas 77204-5001, USA*

A description of how the activity of a population of neurons reflects the structure of its inputs is essential for understanding neural coding. Many studies have examined how inputs determine spiking statistics, while comparatively little is known about membrane potentials. We examine how membrane potential statistics are related to input and spiking statistics. Surprisingly, firing rates and membrane potentials are sensitive to input current modulations in distinct regimes. Additionally, the correlation between the membrane potentials of two uncoupled cells and the correlation between their spike trains reflect input correlations in distinct regimes. Our predictions are experimentally testable, provide insight into the filtering properties of neurons, and indicate that care needs to be taken when interpreting neuronal recordings that reflect a combination of subthreshold and spiking activity.

I. INTRODUCTION

To understand dynamics and information processing in neuronal networks it is important to examine how the inputs to neurons shape their activity. Computational and theoretical approaches to this problem typically focus on spiking activity. However, action potentials are a sparse representation of a cell's response, while the subthreshold membrane potential is continuously modulated by a cell's inputs. In addition, popular recording techniques such as voltage sensitive dyes and local field potentials capture a mixture of subthreshold and spiking activity. While the multivariate statistics of membrane potential traces have been examined experimentally [1–4], a theoretical approach to the problem has not been fully developed [5].

We provide theoretical tools to examine how the statistics of inputs to neurons determine the marginal and joint statistics of their membrane potential activity. This approach also allows us to study how membrane potential statistics are related to spiking statistics. Counter to intuition, we find that current coded signals are reliably reflected by membrane potentials and firing rates in distinct regimes: Firing rates are most sensitive to modulations of a cell's input current when excitation is strong and firing rates are high. In contrast, the mean membrane potential is most sensitive to such modulations when excitation is weak and firing rates low. In addition, we find that when two uncoupled cells receive correlated inputs their spiking correlations and membrane potential correlations are reflective of the correlations between their inputs in distinct regimes.

These findings illuminate some fundamental filtering properties of neurons and have significant implications for the interpretation of different types of experimental recordings. For example, the correlation between two signals obtained from voltage sensitive dyes or local field potentials can exhibit a decrease in correlations when spiking correlations increase.

II. METHODS

We model two cells receiving correlated, stochastic input using a leaky integrate-and-fire (LIF) model. Without loss of generality, we scale and shift the voltage units so that the membrane capacitance is $C_m = 1$ and the leak current has reversal potential at zero. Thus the membrane potential of cell $k = 1,2$ obeys

$$\frac{dV_k}{dt} = -\frac{V_k}{\tau_m} + J_e\, e_k(t) - J_i\, i_k(t) \qquad (1)$$

where $e_1(t) = \sum_j \delta(t - t_{e_1}^j)$ and $e_2(t) = \sum_j \delta(t - t_{e_2}^j)$ are correlated stationary point processes representing excitatory inputs with rate r_e, and similarly for the inhibitory inputs $i_{1,2}(t)$ with rate r_i. The term J_e (J_i) represents the synaptic strength of excitation (inhibition) and τ_m the membrane time constant. Additionally, whenever $V_k(t)$ exceeds threshold at V_{th}, a spike is fired and the membrane potential reset to V_{re}. Output spike trains are given by $s_k(t) = \sum_j \delta(t - t_k^j)$, where t_k^j is the time of the jth spike of cell k. We denote the output firing rates by r_s. For notational convenience, we also define the total input currents $\text{in}_k(t) = J_e\, e_k(t) - J_i\, i_k(t)$ with mean

$$\mu = \langle \text{in}_k(t) \rangle = J_e r_e - J_i r_i.$$

For simplicity, the dynamics and input statistics of the two cells are assumed to be statistically identical in the text, with a general treatment given in the Appendexes.

We quantify the covariance between spike trains and membrane potentials using the cross covariance $C_\kappa(\tau) = \text{cov}[\kappa_1(t), \kappa_2(t + \tau)]$, for $\kappa \in \{s, e, i, \text{in}, V\}$ where $\text{cov}(x,y) = \langle xy \rangle - \langle x \rangle \langle y \rangle$, $\langle \cdot \rangle$ denotes expectation, and processes are assumed stationary and ergodic. The cross covariance between the total input currents is related to the excitatory and inhibitory cross covariances by

$$C_{\text{in}}(\tau) = J_e^2 C_e(\tau) + J_i^2 C_i(\tau) - 2 J_e J_i C_{ei}(\tau), \qquad (2)$$

where $C_{ei}(\tau) = \text{cov}[e_1(t), i_2(t + \tau)] = \text{cov}[i_1(t), e_2(t + \tau)]$. Autocovariances are defined similarly, $A_\kappa(\tau) = \text{cov}[\kappa_k(t), \kappa_k(t + \tau)]$. To quantify the correlation between membrane potentials we normalize the cross covariance to obtain the Pearson normalized cross correlation (hereafter referred to simply as cross correlation)

$$R_V(\tau) = \frac{C_V(\tau)}{A_V(0)} = \frac{\text{cov}[V_1(t), V_2(t + \tau)]}{\sqrt{\text{var}[V_1(t)]\text{var}[V_2(t + \tau)]}}, \qquad (3)$$

which satisfies $|R_V(\tau)| \leqslant 1$ and where $|R_{VV}(0)| = 1$ implies that the membrane potentials are perfectly correlated or anticorrelated [i.e., $V_1(t) = \lambda V_2(t)$].

The Pearson normalized cross correlation between point processes is not defined since they have infinite variance (i.e., $\mathrm{var}[\kappa_k(t)] = \infty$ for $\kappa \in \{e,i,\mathrm{in},s\}$) [6,7]. We instead consider statistics of the spike counts, $N_{\kappa_k}(t_1,t_2) = \int_{t_1}^{t_2} \kappa_k(s)ds$ for $\kappa \in \{\mathrm{in},s,e,i\}$ and $k = 1,2$. Define the normalized spike count variance $\sigma^2(T) = \mathrm{var}[N_{\kappa_k}(t,t+T)]/T$, covariance $\gamma_\kappa(T) = \mathrm{cov}[N_1(t,t+T),N_2(t,t+T)]/T$, and correlation $\rho_\kappa(T) = \gamma_\kappa(T)/\sigma_\kappa^2(T)$.

We next provide a general and intuitive derivation of spiking and membrane potential statistics in the limits of weak and strong excitation. The relation between the two is then examined outside of these limits using a diffusion approximation.

III. WEAK EXCITATION LIMIT

We begin by examining the response properties of a pair of LIFs in a regime where spiking is rare, for instance, when excitation is weaker than the combined current from inhibition and leak ($J_e r_e \ll J_i r_i + V_{\mathrm{th}}/\tau_m$). In this limit we find that the mean membrane potentials reliably reflect the mean input currents. In contrast the cells' firing rates depend only weakly on the mean input current. Additionally, correlations between membrane potentials reflect input correlations, but spiking correlations are nearly zero.

In the limit of weak excitation, the membrane potentials are given by Eq. (1) *without* thresholding, and hence by linearly filtered versions of the inputs. Standard signal processing identities can be used to obtain the membrane potential statistics [8]. The stationary mean of the membrane potentials is proportional to the mean of the input current $\langle V_k \rangle = \mu \tau_m$ so that the gain of the membrane potential is given by

$$\frac{d\langle V_k \rangle}{d\mu} = \tau_m.$$

The autocovariance and cross-covariance functions are obtained by applying a linear filter to the input autocovariance and cross-covariance functions

$$A_V(\tau) = (K * A_{\mathrm{in}})(\tau) \quad \text{and} \quad C_V(\tau) = (K * C_{\mathrm{in}})(\tau), \quad (4)$$

where $K(\tau) = \tau_m e^{-|\tau|/\tau_m}/2$. Thus, the integral correlation coefficient of the input is preserved in the membrane potentials in the sense that

$$\frac{\int_{-\infty}^{\infty} C_V(\tau)d\tau}{\int_{-\infty}^{\infty} A_V(\tau)d\tau} = \frac{\int_{-\infty}^{\infty} C_{\mathrm{in}}(\tau)d\tau}{\int_{-\infty}^{\infty} A_{\mathrm{in}}(\tau)d\tau} = \lim_{T \to \infty} \rho_{\mathrm{in}}(T).$$

The stationary variance is $\mathrm{var}(V_k) = A_V(0) = \int_{-\infty}^{\infty} A_{\mathrm{in}}(\tau)K(\tau)d\tau$ which gives the cross-correlation function [cf. Eq. (3)].

Whereas membrane potential statistics reliably reflect input statistics, the gain of the spike trains and the correlation between spike trains are nearly zero when excitation is weak

$$\frac{dr_s}{d\mu} \approx 0, \quad C_s(\tau) \approx 0 \quad \text{and} \quad \rho_s(T) \approx 0, \quad (5)$$

and asymptotic expansions are known for each [9–12]. The conclusion that spiking correlations vanish in the limit of weak

excitation requires an assumption that input correlations are weak. However, spiking correlations are found to be nearly zero when excitation is weak and input correlations are chosen to be moderate in magnitude [9,10].

The results in this section were obtained by assuming that excitation is weak so that spiking is rare. However, the results are valid any time active spiking conductances have a negligible impact, such as when spiking is suppressed either pharmacologically or by injecting a hyperpolarizing current in experiments [2,3]. See Sec. VI D for further discussion.

IV. STRONG EXCITATION LIMIT

We now examine the response properties of two LIFs when excitation is strong and firing rates are high. In this regime the sensitivity to input currents is reversed: The mean membrane potentials show a weak dependence, but the firing rates reflect the mean input current reliably. Similarly, membrane potential correlations are zero, but spiking correlations reflect input correlations.

When excitation dominates the current across the membrane ($J_e r_e \gg J_i r_i + V_{\mathrm{th}}/\tau_m$), an approximation can be obtained by ignoring the effects of inhibition and leak. Equation (1) is then replaced by the equation for a perfect integrator [9,13]

$$\frac{dV_k}{dt} = J_e e_k(t), \quad (6)$$

with the same threshold and reset conditions. This model is analyzed in Appendix A and we review the results here. Under weak assumptions, we show that the bivariate distribution of $(V_1(t), V_2(t + \tau))$ is uniform, generalizing the univariate result in Ref. [14]. We also assume that $V_{\mathrm{th}} - V_{\mathrm{re}}$ is an integer multiple of J_e, which simplifies the exposition, but does not significantly change the results.

The mean membrane potential is given by $\langle V_k \rangle = (V_{\mathrm{th}} + V_{\mathrm{re}})/2$. Thus, the gain of the membrane potentials is zero in this limit,

$$\frac{d\langle V_k \rangle}{d\mu} = 0.$$

Two random variables whose joint distribution is uniform are necessarily independent, and therefore $V_1(t)$ is independent from $V_2(t + \tau)$, and so

$$C_V(\tau) = R_V(\tau) = 0 \quad (7)$$

for all τ. It is worth noting that this result is not valid when the cells' inputs are perfectly correlated since identical inputs imply that the bivariate membrane potential process is not ergodic on its state space.

Whereas the gain and correlation of the membrane potentials are zero in the limit of strong excitation, the spike trains reliably reflect the inputs. The firing rate is given by $r_s = r_e/\theta = \mu/(V_{\mathrm{th}} - V_{\mathrm{re}})$ where $\theta = (V_{\mathrm{th}} - V_{\mathrm{re}})/J_e$ is the number of inputs required to reach threshold from reset. This gives the gain

$$\frac{dr_s}{d\mu} = (V_{\mathrm{th}} - V_{\mathrm{re}})^{-1}.$$

Perhaps counterintuitively, the membrane potentials for this model are independent, but the output spike trains are correlated. This is possible because the times at which the membrane potentials jump are correlated even though the states that they occupy are not. To see this, suppose that $C_e(\tau) > 0$ and that cell 1 spikes at time t. Then cell 1 necessarily received an excitatory input at time t. Although conditioning on a spike in cell 1 does not affect the distribution of $V_2(t + \tau)$, the fact that cell 1 received an input at time t increases the probability that cell 2 receives an input near time $t + \tau$ since $C_e(\tau) > 0$. This in turn increases the probability that cell 2 spikes near time $t + \tau$. In Appendix A, this argument is used to derive the output cross-covariance function

$$C_s(\tau) = \theta^{-2} C_e(\tau) = (V_{th} - V_{re})^{-2} C_{in}(\tau). \tag{8}$$

Spike count statistics over large time windows are known in closed form for this model [9,15]. Variances and covariances are scaled, $\lim_{T\to\infty} \sigma_s^2(T) = (V_{th} - V_{re})^{-2} \lim_{T\to\infty} \sigma_{in}^2(T)$ and $\lim_{T\to\infty} \gamma_s(T) = (V_{th} - V_{re})^{-2} \lim_{T\to\infty} \gamma_{in}(T)$ so that spiking correlations over large time windows equal input correlations

$$\lim_{T\to\infty} \rho_s(T) = \lim_{T\to\infty} \rho_{in}(T).$$

However, spike count correlations over small windows are reduced since, to first order in T,

$$\rho_s(T) \approx \frac{C_s(0)}{r_s} T = \frac{\theta^{-2} C_e(0)}{\theta^{-1} r_e} T \approx \theta^{-1} \rho_{in}(T).$$

The model defined by Eq. (6) is a simplification of realistic neuronal dynamics, even when excitation is strong. However, we show next that these results accurately predict the statistics of two LIFs receiving strong excitation.

V. ANALYSIS OF THE DIFFUSION APPROXIMATION

The model given by Eq. (1) is difficult to analyze outside of the two limits discussed above, so we instead consider a diffusion approximation

$$\frac{dV_k}{dt} = -\frac{V_k}{\tau_m} + \mu + \sqrt{2D}\, \eta_k(t). \tag{9}$$

Here, $\eta_1(t)$ and $\eta_2(t)$ are unbiased Gaussian noise with $\langle \eta_k(t) \eta_k(t + \tau) \rangle = \delta(\tau)$ and $2D\langle \eta_1(t)\eta_2(t + \tau)\rangle = C_{in}(\tau)$. The parameter, $D = (J_e^2 r_e + J_i^2 r_i)/2$, is the effective diffusion coefficient of the input current. This approximation is valid when $e_k(t)$ and $i_k(t)$ are independent Poisson processes [but $e_1(t)$ and $i_2(t)$ need not be independent] and $J_e, J_i \ll V_{th} - V_{re}$. Although the inputs are assumed to be Poissonian, their pairwise cross covariances need not be delta functions [16,17]. See [14,18–20] for a more in-depth look at the validity of the diffusion approximation.

Univariate and bivariate spiking statistics for this model have been studied extensively and the univariate moments are known in closed form Refs. [21,22], but the statistics of the membrane potentials have received comparatively little attention. Below, we use the Fokker-Planck formulation from Refs. [23,24] to derive membrane potential statistics in terms of the input parameters and the output spiking statistics.

A. Stationary mean and variance of the membrane potentials

In Appendix B, we derive the steady-state mean and variance of the membrane potentials

$$\langle V_k \rangle = \tau_m[\mu - (V_{th} - V_{re})r_s], \tag{10}$$

$$\mathrm{var}(V_k) = \tau_m D - \left[\left(V_{th}^2 - V_{re}^2\right)/2 - \tau_m\mu(V_{th} - V_{re})\right]\tau_m r_s \\ - (V_{th} - V_{re})^2 \tau_m^2 r_s^2. \tag{11}$$

The stationary firing rate r_s and the stationary density P_0 are known in closed form and can also be obtained by solving a boundary value problem [7,23,25].

The mean and variance of $V_k(t)$ can also be obtained by integrating the stationary density, but Eqs. (10) and (11) are easier to evaluate and have an intuitive interpretation: Taking $r_s \to 0$ gives the mean and variance in the weak excitation limit (compare to Sec. III). The remaining terms quantify the effect of thresholding in terms of the firing rate.

The mean membrane potential and firing rate are shown as a function of r_e in Fig. 1(a). When r_e is small, $r_s \approx 0$ and $\langle V_k \rangle$ increases approximately linearly with r_e, consistent with the discussion in Sec. III. When r_e is larger, r_s increases
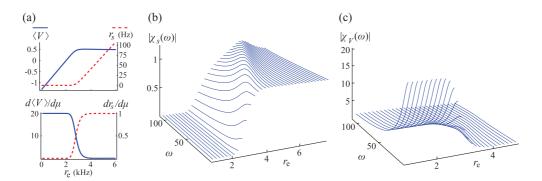

FIG. 1. (Color online) (a) Firing rate (r_s, dashed red line, top), mean membrane potential ($\langle V \rangle$, solid blue line, top) and gains ($dr_s/d\mu$, dashed red line, bottom; $d\langle V \rangle/d\mu$, solid blue line, bottom) as functions of the excitatory input rate r_e. (b) Susceptibility magnitude of the firing rate. (c) Susceptibility magnitude of the mean membrane potential. As the level of excitation increases, firing rates become more sensitive and membrane potentials become less sensitive to perturbations. In all plots $r_i = 2$ KHz and $\tau_m = 20$ ms. Voltage is scaled so that $V_{re} = 0$ and $V_{th} = 1$ with $J_e = J_i = 1/30$. Mean membrane potential has units $(V_{th} - V_{re})^{-1}$, ω has units Hz, and susceptibility functions have units $(V_{th} - V_{re})^{-1}$ for χ_s and ms for χ_V.

approximately linearly with r_e and $\langle V_k \rangle \approx (V_{\text{th}} + V_{\text{re}})/2$, consistent with Sec. IV.

B. Membrane potentials and firing rates are sensitive to input current modulations in distinct regimes

We now examine the sensitivity of the firing rate and mean membrane potential to modulations of the input current for the diffusion approximation. This extends the results in the limiting cases in Secs. III and IV, where we found that the firing rate and mean membrane potential are sensitive to modulations of the input current in distinct regimes.

The gain of the membrane potential is given by taking the derivative of Eq. (10) with respect to μ to give

$$\frac{d\langle V_k \rangle}{d\mu} = \tau_m \left(1 - (V_{\text{th}} - V_{\text{re}})\frac{dr_s}{d\mu} \right). \tag{12}$$

This expression and Fig. 1(a) indicate a dichotomy between the regimes where r_s and $\langle V_k \rangle$ depend sensitively on the input bias: When excitation is weak, the gain of the firing rates is nearly zero and the gain of the membrane potentials is maximal,

$$\frac{dr_s}{d\mu} \approx 0 \quad \text{and} \quad \frac{d\langle V_k \rangle}{d\mu} \approx \tau_m,$$

consistent with the results in Sec. III. When excitation is strong, the gain of the firing rate is maximal and the gain of the membrane potentials is approximately zero,

$$\frac{dr_s}{d\mu} \approx (V_{\text{th}} - V_{\text{re}})^{-1} \quad \text{and} \quad \frac{d\langle V_k \rangle}{d\mu} \approx 0,$$

consistent with the results in Sec. IV. Equation (12) interpolates these two regimes.

We now use linear response theory to analyze the sensitivity of the neuronal responses to dynamic modulations of the input current by examining the response to the bias current $\mu(t) = \mu_0 + \epsilon e^{i\omega t}$ in Eq. (9). Using a complex perturbation allows us to derive the amplitude and phase shift simultaneously [23].

The susceptibility functions $\chi_V(\omega)$ and $\chi_s(\omega)$ of the mean membrane potential and firing rate are defined by the asymptotic relations [26]

$$\langle V_k(t) \rangle = \langle V_0 \rangle + \epsilon \, \chi_V(\omega) e^{i\omega t} + o(\epsilon),$$
$$r_s(t) = r_0 + \epsilon \, \chi_s(\omega) e^{i\omega t} + o(\epsilon),$$

where $\langle V_0 \rangle$ and r_0 are the stationary mean membrane potential and firing rate when $\epsilon = 0$.

The function $\chi_s(\omega)$ is known in closed form and its properties have been studied extensively [7,23,25]. In Appendix B, we derive the membrane potential susceptibility in terms of $\chi_s(\omega)$ as

$$\chi_V(\omega) = \frac{\tau_m}{1 + i\omega\tau_m}[1 - (V_{\text{th}} - V_{\text{re}})\chi_s(\omega)]. \tag{13}$$

Note that taking $\omega = 0$ in Eq. (13) recovers Eq. (12) since $\chi_s(0) = dr_s/d\mu$ and $\chi_V(0) = d\langle V_k \rangle/d\mu$. Taking the norm squared on either side of Eq. (13) relates the sensitivity of the firing rate and membrane potential to modulations of the input current at frequency ω,

$$|\chi_V(\omega)|^2 = \widetilde{K}(\omega)|1 - (V_{\text{th}} - V_{\text{re}})\chi_s(\omega)|^2, \tag{14}$$

where $\widetilde{K}(\omega) = \int_{-\infty}^{\infty} K(t)e^{-i\omega t}dt = \tau_m^2/(1 + \tau_m^2\omega^2)$ is the Fourier transform of the kernel $K(t)$ from Sec. III.

Figures 1(b) and 1(c) compare the amplitude of the spiking and membrane potential susceptibility. When excitation is weak

$$|\chi_s(\omega)| \approx 0 \quad \text{and} \quad |\chi_V(\omega)| \approx \sqrt{\widetilde{K}(\omega)}.$$

When excitation is strong

$$|\chi_s(\omega)| \approx (V_{\text{th}} - V_{\text{re}})^{-1} \quad \text{and} \quad |\chi_V(\omega)| \approx 0.$$

Thus, spiking and subthreshold dynamics reliably reflect dynamic input modulations in distinct regimes.

C. Membrane potential and spiking correlations reflect input correlations in distinct regimes

We now examine the spiking and membrane potential correlations using the diffusion approximation. Confirming the results in Secs. III and IV, we find that spiking and membrane potential correlations reflect input correlations in distinct regimes.

When input correlations are weak, linear response theory can be used to derive the following approximation of the output cross-covariance function [10,11,27,28]

$$\widetilde{C}_s(\omega) \approx |\chi_s(\omega)|^2 \, \widetilde{C}_{\text{in}}(\omega) \tag{15}$$

and, by an identical argument,

$$\widetilde{C}_V(\omega) \approx |\chi_V(\omega)|^2 \, \widetilde{C}_{\text{in}}(\omega). \tag{16}$$

The cross covariances can then be obtained by inverting the Fourier transform. Combining Eq. (14) with Eqs. (15) and (16) provides insight into the relationship between spiking and subthreshold correlations. When excitation is weak

$$\widetilde{C}_s(\omega) \approx 0 \quad \text{and} \quad \widetilde{C}_V(\omega) \approx \widetilde{K}(\omega)\widetilde{C}_{\text{in}}(\omega),$$

consistent with the results in Sec. III [see Eqs. (4) and (5)]. When excitation is strong

$$\widetilde{C}_s(\omega) \approx (V_{\text{th}} - V_{\text{re}})^{-2}\widetilde{C}_{\text{in}}(\omega) \quad \text{and} \quad \widetilde{C}_V(\omega) \approx 0,$$

consistent with the results in Sec. IV [see Eqs. (7) and (8)]. Equation (14) interpolates these two limits. Figure 2 shows how $C_V(\tau)$ and $C_s(\tau)$ change with r_e and confirms that the cross covariance between the membrane potentials and the cross covariance between the spike trains reflect input correlations in opposite regimes.

Cross covariances are not normalized to account for noise magnitude. In Fig. 3, we show how spike count correlations and normalized membrane potential cross correlations change with firing rate when r_e is increased. In general, spike count correlations increase with r_e and r_s, while membrane potential cross correlations decrease, consistent with recordings from the rat hippocampus [4]. Figure 3 shows that the linear response and diffusion approximations provide an excellent agreement to results obtained via direct simulation of Eq. (1).

So far, we have examined how changes in r_e affect correlations. In Fig. 4, we show that the overall trends are the same if r_i is varied simultaneously, but the decrease in membrane potential correlations is less dramatic.
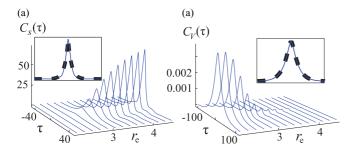
(a) $C_s(\tau)$

(a) $C_V(\tau)$

FIG. 2. (Color online) (a) Cross covariance between spike trains as r_e increases. Inset compares linear response calculation (solid) to the strong excitation limit [dashed line, from Eq. (8)] when $r_e = 4.5$ KHz. (b) Cross covariance between membrane potentials as r_e increases. Inset compares linear response calculation (solid) to the weak excitation limit [dashed line, from Eq. (4)] when $r_e = 2.15$ KHz. Parameters are the same as in Fig. 1 with input cross covariances $C_e(\tau) = \rho_{\rm in} r_e e^{-|\tau|/\tau_{\rm in}}/\tau_{\rm in}$, $C_i(\tau) = \rho_{\rm in} r_i e^{-|\tau|/\tau_{\rm in}}/\tau_{\rm in}$, and $C_{ei}(\tau) = 0$ so that, from Eq. (2), $C_{\rm in}(\tau) = \rho_{\rm in} D e^{-|\tau|/\tau_{\rm in}}/\tau_{\rm in}$ with input correlation magnitude $\rho_{\rm in} = 0.1$ and time scale $\tau_{\rm in} = 5$ ms. Axes have units ms for τ, KHz for r_e, Hz^2 for $C_s(\tau)$, and $(V_{\rm th} - V_{\rm re})^2$ for $C_V(\tau)$. Firing rates vary in range from 0.1 to 58 Hz.

D. Correlation time scales

In Fig. 2, the time scale of $C_s(\tau)$ when excitation is strong appears faster than the time scale of $C_V(\tau)$ when excitation is weak. The membrane potential cross covariance is a low-pass filtered version on the input cross covariance [see Eq. (4) and also compare Eq. (16) with Fig. 1(c)]. On the other hand, the input cross covariance is transferred faithfully to the spiking cross covariance when excitation is strong [see Eq. (8) and also compare Eq. (15) with Fig. 1(b)]. Thus, whenever the time scale of $C_{\rm in}(\tau)$ is faster than the membrane time constant ($\tau_{\rm in} < \tau_m$), $C_s(\tau)$ will appear to decay faster than $C_V(\tau)$. However, the *tails* of $C_s(\tau)$ and $C_V(\tau)$ actually decay at the same exponential rate as $\tau \to \infty$ (not pictured, but see [27]).

This phenomenon can be explained intuitively by noting that $C_s(\tau)$ is determined by two interacting mechanisms when input correlations are positive: (1) input correlations increase the likelihood that both $V_1(t)$ and $V_2(t + \tau)$ are near threshold and (2) an input that pushes cell 1 over threshold near time t increases the likelihood that cell 2 receives an input at time $t + \tau$. The effect of the first mechanism on $C_s(\tau)$ decays asymptotically like $e^{-\tau/\tau_m}$, whereas the effect of the second mechanism decays like $C_e(\tau)$. Since the membrane potentials

(a) $\rho_s(t)$

(b) $R_V(t)$

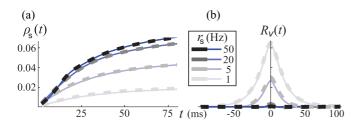| r_s (Hz)	
	50
	20
	5
	1

FIG. 3. (Color online) (a) Spike count correlations and (b) normalized membrane potential cross correlation at various firing rates (see inset). Linear response approximations (solid line) are compared to simulations with Poisson inputs (dashed line). Firing rates were modulated by changing r_e. All other parameters are as in Fig. 2.
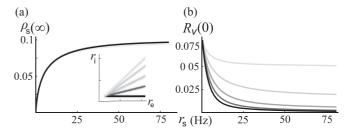

(a) $\rho_s(\infty)$

(b) $R_V(0)$

FIG. 4. (a) Spike count correlation over large time windows and (b) peak membrane potential correlation plotted against firing rate as r_e and r_i vary along linear paths: $r_e - 500\,{\rm Hz} = \alpha(r_i - 500\,{\rm Hz})$ for different slopes α (see inset). All other parameters are as in Fig. 2.

are nearly independent when excitation is strong, the first mechanism has a much smaller effect in this regime and the second mechanism determines the shape of the peak of $C_s(\tau)$. However, the first mechanism dominates in the tail of $C_s(\tau)$ since its effect decays more slowly.

VI. DISCUSSION

We derived a number of results that relate subthreshold membrane potential statistics of two uncoupled integrate-and-fire neurons to their spiking statistics and to the statistics of their inputs. We found that a cell's firing rate and mean membrane potential are sensitive to modulations of its input currents in opposite regimes. We additionally showed that correlations between the cells' spike trains and membrane potentials also reflect input correlations in opposite regimes. Thus, care must be taken when interpreting the marginal and joint statistics of underlying cell responses from experimental recordings.

When examining spiking and membrane potential correlations, we only considered a pair of uncoupled cells. Synaptic and electrical coupling will impact spike train and membrane potential correlations. Linear response theory could be used to extend our methods [27,28].

A. Comparing spiking and membrane potential correlations when input correlations change

In all of the results plotted above, we fixed input correlations while varying the excitatory and inhibitory input rates r_e and r_i. This assumption helped isolate changes in spiking and membrane potential correlations that were due to nonlinear neuronal filtering. However, *in vivo* input correlations can change with stimulus and behavioral states. Thus, one should not necessarily expect that input correlations remain fixed as other parameters change.

As discussed in Sec. V, spiking and membrane potential correlations generally change oppositely with changes in r_e and r_i. However, they both increase with an increase of input correlations. In Fig. 5, we consider a situation where spiking and membrane potential correlations are computed for randomly sampled points in input parameter space. When r_e and r_i are drawn from wide distributions and the magnitude of input correlations is drawn from narrower distributions [Fig. 5(a)], spiking and membrane potentials vary inversely with one another. However, when r_e and r_i are drawn from narrow distributions and the magnitude of input correlations
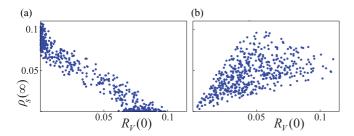
FIG. 5. (Color online) Spike count correlation over large time windows versus peak membrane potential correlation for 500 randomly generated excitatory and inhibitory input rates and correlations. (a) Input rates were drawn from wide uniform distributions ($r_e \in [2,4]$ KHz and $r_i \in [0,1.75]$ KHz) and input correlations from narrow uniform distributions ($\rho_{ee} \in [0.15,0.2]$, $\rho_{ii} \in [0.15,0.2]$, and $\rho_{ei} = 0$). (b) Input rates were drawn from narrower uniform distributions ($r_e \in [2.2,2.4]$ KHz and $r_i \in [1.3,1.4]$ KHz) and input correlations from wider uniform distributions ($\rho_{ee} \in [0,0.2]$, $\rho_{ii} \in [0,0.2]$, and $\rho_{ei} = 0$). Parameters are the same as in Fig. 2 except input cross covariances are $C_e(\tau) = \rho_{ee} r_e e^{-|\tau|/\tau_{in}}/\tau_{in}$, $C_i(\tau) = \rho_{ii} r_i e^{-|\tau|/\tau_{in}}/\tau_{in}$, and $C_{ei}(\tau) = 0$.

is drawn from wider distributions [Fig. 5(a)], spiking and membrane potentials vary together. Thus, despite our results, spiking and membrane potential correlations need not change oppositely with input statistics in situations where input correlations are modulated.

B. A spiking model with active conductances

The LIF model we analyzed has the advantage that subthreshold activity is easily separated from spiking activity. However, experimental recordings, such as those of local field potentials or the light emitted by voltage sensitive dyes, often represent a combination of spiking and subthreshold activity. Additionally, the sharp threshold and lack of active currents in the LIF can yield anomalous response properties [29]. To test whether our results hold for a spiking model with active conductances, we used an exponential integrate-and-fire (EIF) model in which the membrane potential is held at 40 mV for 1.5 ms at each spike. We refer to this model as a "spiking EIF."

A representative output is shown in Fig. 6(c) and the model is fully described in Appendix C.

Figure 6(a) shows the mean membrane potential and an estimate of the gain for this model as a function of r_e. The estimated gain decreases for large r_e, but does not approach zero. This is likely due to the contribution of spikes to the mean membrane potential. Figure 6(b) shows that correlations between the membrane potential traces of two spiking EIF cells decrease with r_e, similar to the LIF.

C. Implications for pooled recordings

Recordings of local field potentials and voltage sensitive dye signals can represent the pooled activity of large populations of cells. The correlation between two such pooled signals is generally larger than the correlations between the activity individual cells in the recorded populations [30–35]. We model the pooled signals by summing the individual membrane potentials $X_k(t) = \sum_{j=1}^{n} V_j^k(t), k = 1,2$. If the populations are homogeneous, then the cross correlation between the summed activities is given by Ref. [34]

$$R_X(\tau) = \frac{R_V(\tau)}{R_V(0) + \frac{1}{n}[1 - R_V(0)]} = \frac{R_V(\tau)}{R_V(0)} + \mathcal{O}(1/n). \quad (17)$$

If the population is heterogeneous or if some cells' membrane potentials contribute more strongly to the pooled signals, $R_V(\tau)$ can be replaced by a weighted average of the cross correlations in Eq. (17) [34]. For large populations ($n \gg 1$), this amplification of correlations can mask the decrease in correlations shown in Fig. 6(b) since even when individual cells are weakly correlated, the pooled signals will be strongly correlated. This effect is illustrated for the spiking EIF model in Fig. 6(d): Even though the correlation between individual membrane potentials decreases quickly and dramatically with r_e, the correlation between two pooled recordings decreases only modestly and slowly with r_e. For larger n, the decrease is reduced even further.
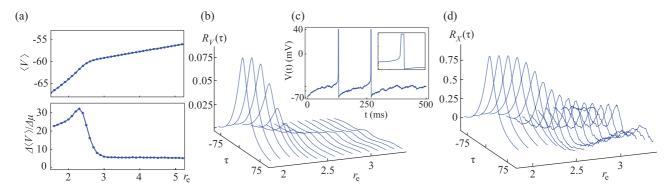

FIG. 6. (Color online) (a) Mean membrane potential and an approximation to the gain (found by taking $\Delta\langle V \rangle/\Delta\mu$ for the points sampled) for the spiking EIF model as a function of r_e. Dots show sampled points, which are interpolated linearly. (b) Membrane potential cross correlation for a spiking EIF model plotted for various values of r_e. (c) A sample voltage trace (taken at $r_e = 2.7$ KHz) and the trajectory of a single spike for the spiking EIF. (d) Cross correlations between two pooled recordings of 200 membrane potential traces, obtained by applying Eq. (17) to the cross correlations in (b) with $n = 200$. Note that correlations are at least an order of magnitude larger here than in (b) due to pooling. Input parameters are as in Fig. 2.

D. Comparison with experimental results

Experimentally, spiking correlations were found to increase while membrane potential correlations decrease with an increase in firing rate associated at the onset of seizure-like activity [4]. This is consistent with the results in Sec. V C. However, we note that membrane potential correlations in [4] were computed by deleting a few milliseconds surrounding each spike from the membrane potential traces. It is not clear what effect this deletion has on the computed correlations and whether it compromises the applicability of our results to their findings.

In Ref. [2], membrane potential cross correlations were compared to spiking cross covariances *in vivo*. The membrane potential cross correlations were obtained while the cells were hyperpolarized by a constant injected current to prevent spiking. Cross covariances between the spike trains were obtained while the cells were depolarized by a constant injected current to promote spiking. These two conditions are analogous to the weak and strong excitation conditions discussed above: Our results are preserved when "weak excitation" is replaced by "strong hyperpolarizing current" and "strong excitation" is replaced by "strong depolarizing current." The authors found that membrane potential cross correlations in the hyperpolarized state have a longer time scale than spiking correlations in the depolarized state, consistent with our results in Sec. V D.

Membrane potential cross correlations were also reported in Ref. [3] under hyperpolarized and depolarized conditions, but spiking was pharmacologically suppressed in these recordings. Since the decrease of $R_V(\tau)$ with r_e reported above depends on a threshold and reset, our results do not apply when spiking is suppressed.

Integrate-and-fire (IF) models provide a minimal description of membrane and spiking dynamics. However, the behavior of networks of IF neurons is frequently in good agreement with biological neuronal networks [28,36]. We therefore expect that our results can provide further insight into the dynamics of neuronal networks.

ACKNOWLEDGMENTS

APPENDIX A: ANALYSIS OF THE STRONG EXCITATION LIMIT

We analyze the model considered in Sec. IV whose membrane potential is defined by Eq. (6). Here we consider the general case and do not assume that the cells are dynamically identical or that they receive statistically identical inputs. This introduces the need for subscripted notation (e.g., $V_{th,k}$, $r_{e,k}$, etc. for $k = 1,2$).

After being reset to $V_k(t) = V_{re,k}$, the membrane potential is incremented by $J_{e,k}$ at each input spike and therefore remains in the state space $\Gamma_k = \{V_{re,k}, V_{re,k} + J_{e,k}, \ldots, V_{re,k} + \theta_k J_{e,k}\}$ where $\theta_k = \lfloor (V_{th,k} - V_{re,k})/J_{e,k} \rfloor$ is the number of input spikes to bring cell k from reset to threshold and $\lfloor \cdot \rfloor$ gives the integer

part of the argument. Thus, the bivariate membrane potential process $(V_1(t), V_2(t))$ has state space $\Gamma = \Gamma_1 \times \Gamma_2$.

Cell k spikes after every θ excitatory inputs. Thus, the firing rate is easily seen to be $r_{s,k} = r_{e,k}/\theta_k$.

The membrane potential at any two points in time are related by

$$V_k(t_1) = V_k(t_0) \oplus_k J_{e,k} N_{e_k}(t_0,t_1), \tag{A1}$$

where $N_{e_k}(t_0,t_1) = \int_{t_0}^{t_1} e_k(t)dt$ is the number of excitatory inputs in the open interval (t_0,t_1) and $\oplus_k$ represents modular addition on the discrete state space Γ_k.

We now show that the membrane potentials sampled at any two points in time have a bivariate uniform distribution.

Theorem 1. Consider the two-cell IF model defined by Eq. (6) with resets at $V_{re,k}$ and thresholds at $V_{th,k}$. Assume that the membrane potential process is ergodic with finite memory in the sense that there exists a steady-state probability mass function $p : \Gamma \times \mathbb{R}^2 \to \mathbb{R}^+$ such that

$$
\begin{aligned}
p(v_1,v_2;t_1,t_2) &= \lim_{t \to \infty} \Pr[V_1(t_1 + t) = v_1, V_2(t_2 + t) \\
&= v_2 | V_1(0) = u_1, V_2(0) = u_2]
\end{aligned}
$$

and $p(v_1,v_2;t_1,t_2) > 0$ for all $t_1,t_2 \in \mathbb{R}^+$ and $(v_1,v_2),(u_1,u_2) \in \Pi$. Then p is uniform with

$$p(v_1,v_2;t_1,t_2) = (\theta_1\theta_2)^{-1}$$

for all $t_1,t_2 \in \mathbb{R}^+$ and $(v_1,v_2) \in \Pi$.

Proof. Suppose $(v_1,v_2),(w_1,w_2) \in \Pi$ and $t_1,t_2 \in \mathbb{R}^+$. From Eq. (A1), the event that $(V_1(t_1 + t), V_2(t_2 + t)) = (v_1,v_2)$ given $(V_1(0), V_2(0)) = (0,0)$ has the same probability as the event that $J_{e,k}(N_{e_k}(t_k + t) \bmod \theta_k) = V_k(t_k + t)$ for $k = 1,2$. By the same reasoning, this is in turn has the same probability as the event that $(V_1(t_1 + t), V_2(t_2 + t)) = (w_1,w_2)$ given $(V_1(0), V_2(0)) = (w_1 \oplus_1 -v_1, w_2 \oplus_2 -v_2)$. Thus,

$$
\begin{aligned}
p(v_1,v_2;t_1,t_2) &= \lim_{t \to \infty} \Pr[V_1(t_1 + t) = v_1, V_2(t_2 + t) \\
&= v_2 | V_1(0) = 0, V_2(0) = 0] \\
&= \Pr[V_1(t_1 + t) = w_1, V_2(t_2 + t) = w_2 \\
&\quad | V_1(0) = w_1 \oplus_1 -v_1, V_2(0) = w_2 \oplus_2 -v_2] \\
&= p(w_1,w_2;t_1,t_2)
\end{aligned}
$$

and therefore p is uniform. Since p is a probability mass function with respect to its first two arguments, we may conclude that

$$p(v_1,v_2;t_1 t_2) = \frac{1}{\text{card}(\Pi)} = \frac{1}{\theta_1\theta_2}.$$

∎

The assumption of ergodicity with finite memory made in Theorem 1 essentially assures that the bivariate distribution of the membrane potentials approaches a steady state that does not depend on initial conditions. We expect this assumption to hold when inputs are not perfectly correlated and do not have infinite memory. For example, if inputs are delta-correlated Poisson processes, this assumption is straightforward to verify. However, the assumption can be violated by inputs that exhibit infinite-time-scale deterministic trends. For example, if the input to one cell is perfectly periodic (an input spike arriving every T ms) with a random and uniformly distributed phase,

then the input process is stationary, but the assumption is violated.

Since the components of a bivariate uniform distribution are independent, we may conclude from Theorem 1 that $V_1(t_1)$ is independent from $V_2(t_2)$ for any times t_1 and t_2. From this fact, we can derive the output cross-covariance function as follows. First note that the cross covariance can be written as [37]

$$C_s(\tau) = \lim_{\delta \to 0} \delta^{-2} \Pr[N_{s_1}(t, t + \delta) > 0, N_{s_2}(t + \tau, t + \tau + \delta) > 0] - r_{s,1} r_{s,2}. \quad \text{(A2)}$$

Now note that a spike occurs in $s_k(t)$ at time t_0 only if an excitatory input arrives [from $e_k(t)$] at time t_0 and $V_k(t_0) \in [V_{\text{th},k} - J_{e,k}, V_{\text{th}}]$. Thus, Eq. (A2) can be rewritten as

$$C_s(\tau) = \lim_{\delta \to 0} \delta^{-2} \Pr[V_1(t) \in [V_{\text{th}} - J_e, V_{\text{th}}], N_{e_1}(t, t + \delta) > 0, V_2(t + \tau) \in [V_{\text{th}} - J_e, V_{\text{th}}], N_{e_2}(t + \tau, t + \tau + \delta) > 0] - r_{s,1} r_{s,2}. \quad \text{(A3)}$$

Finally, since the membrane potentials are independent and uniformly distributed, this becomes

$$C_s(\tau) = (\theta_1 \theta_2)^{-1} \Big(\lim_{\delta \to 0} \delta^{-2} \Pr\big[N_{e_1}(t, t + \delta) > 0, N_{e_2}(t + \tau, t + \tau + \delta) > 0 \big] - r_{e,1} r_{e,2} \Big)$$

$$= (\theta_1 \theta_2)^{-1} C_e(\tau).$$

In the text, we assume that $V_{\text{th},k} - V_{\text{re},k}$ is an integer multiple of $J_{e,k}$ for $k = 1,2$. This assumption can be made without loss of generality since when it is not met $V_{\text{th},k}$ can be replaced by $V_{\text{re},k} + \theta_k J_{e,k}$ without affecting the dynamics. Under this assumption, $\theta_k = (V_{\text{th},k} - V_{\text{re},k})/J_{e,k}$ and therefore $r_{s,k} = J_{e,k} r_{e,k}/(V_{\text{th},k} - V_{\text{re},k}) = \mu_k/(V_{\text{th},k} - V_{\text{re},k})$ and $C_s(\tau) = (\theta_1 \theta_2)^{-1} C_e(\tau) = (V_{\text{th},1} - V_{\text{re},1})^{-1}(V_{\text{th},2} - V_{\text{re},2})^{-1} C_{\text{in}}(\tau)$. Additionally, the mean membrane potential is given by $\langle V_k \rangle = (V_{\text{th},k} + V_{\text{re},k})/2$ since its distribution is uniform on Γ_k.

APPENDIX B: DERIVATION OF MEMBRANE POTENTIAL STATISTICS FOR THE DIFFUSION APPROXIMATION

We now derive the expressions from Sec. V that relate membrane potential statistics of the diffusion approximation to the firing rate and susceptibility. Since we focus on univariate statistics here, we omit subscripts that indicate neuron number [i.e., we use $V(t)$ in place of $V_k(t)$]. Though we do not discuss lower barriers on the membrane potentials in the text, we allow for the possibility of a reflecting barrier at some $V_{\text{lb}} \leqslant V_{\text{re}}$ in our calculations below. The unbounded case can be recovered by setting $V_{\text{lb}} = -\infty$. However, our numerical calculations require a finite lower barrier. In all figures, the lower barrier was set so low that it did not significantly affect the statistics (see Appendix D).

Much of our analysis uses standard properties of bilateral Laplace transforms, defined by

$$\mathcal{L}[f(x)](s) = \widehat{f}(s) = \int_{-\infty}^{\infty} f(x) e^{-sx} dx.$$

When X is a random variable with density f, then $\widehat{f}(0) = 1$, $\widehat{f}'(0) = \langle X \rangle$, and $\widehat{f}''(0) = \langle X^2 \rangle$.

From Refs. [23,24], the stationary density and probability flux, $P_0(v)$ and $J_0(v)$, of $V(t) = V_k(t)$ from Eq. (9) obey

$$-\frac{\partial P_0}{\partial v} = \frac{1}{D}[(v/\tau_m - \mu)P_0 + J_0]$$

$$-\frac{\partial J_0}{\partial v} = r_s[\delta(V - V_{\text{th}}) - \delta(V - V_{\text{re}})].$$

We first derive the stationary mean of the membrane potential. Taking the bilateral Laplace transform on either side of these equations gives

$$\widehat{P}_0 = \frac{1}{D}\left(\frac{1}{\tau_m}\frac{\partial \widehat{P}_0}{\partial s} - \mu \widehat{P}_0 + \widehat{J}_0\right)$$

$$s\widehat{J}_0 = r_s(e^{V_{\text{th}}s} - e^{V_{\text{re}}s}),$$

which can be solved algebraically to obtain

$$\frac{\partial \widehat{P}_0}{\partial s} = \tau_m(\mu + sD)\widehat{P}_0 - \frac{\tau_m}{s}(e^{V_{\text{th}}s} - e^{V_{\text{re}}s})r_s. \quad \text{(B1)}$$

Taking $s \to 0$ yields an expression for the the mean membrane potential, given in Eq. (10).

To derive the variance of the membrane potentials, first differentiate Eq. (B1) to obtain

$$\frac{\partial^2 \widehat{P}_0}{\partial s^2} = \tau_m \frac{\partial \widehat{P}_0}{\partial s}(\mu + sD) + \tau_m D \widehat{P}_0$$

$$- \frac{\tau_m}{s^2}[e^{V_{\text{th}}s}(sV_{\text{th}} - 1) - e^{V_{\text{re}}s}(sV_{\text{re}} - 1)]r_s$$

which, upon taking $s \to 0$, gives

$$\langle V^2 \rangle = \tau_m\big(\mu\langle V \rangle + D - \tfrac{1}{2}\big(V_{\text{th}}^2 - V_{\text{re}}^2\big)r_s\big),$$

which, using Eq. (10), yields the expression for $\text{var}[V(t)] = \langle V^2 \rangle - \langle V \rangle^2$ given in Eq. (11).

Similar methods can be used to derive the response properties of the mean membrane potential. Given a periodically perturbed bias $\mu(t) = \mu_0 + \epsilon e^{i\omega t}$, the probability density can be written to first order in ϵ as $P(v,t) = P_0(v) + \epsilon P_1(v)e^{i\omega t} + o(\epsilon)$ and similarly for the flux $J(v,t) = J_0(v) + \epsilon J_1(v)e^{i\omega t}$ where P_0 and J_0 are the solutions when $\epsilon = 0$ (see above). Isolating the first-order terms of the time-dependent Fokker-Planck equation gives [23,24]

$$-\frac{\partial P_1}{\partial v} = \frac{1}{D}[(v/\tau_m - \mu_0)P_1 + J_1 - P_0],$$

$$-\frac{\partial J_1}{\partial v} = i\omega P_1 + \chi_s(\omega)[\delta(v - V_{\text{th}}) - \delta(v - V_{\text{re}})], \quad \text{(B2)}$$

where $\chi_s(\omega)$ is the susceptibility of the firing rate, which satisfies $r_s(t) = r_0 + \epsilon \chi_s(\omega)e^{i\omega t}$, where r_0 is the firing rate when $\epsilon = 0$. The susceptibility $\chi_V(\omega)$ of the mean membrane potential is defined by $\langle V(t) \rangle = \langle V_0 \rangle + \epsilon \chi_V(\omega)e^{i\omega t} + o(\epsilon)$, where $\langle V_0 \rangle = \int_{V_{\text{lb}}}^{V_{\text{th}}} v P_0(v)dv$ is the stationary mean membrane potential when $\epsilon = 0$ and is given by Eq. (10). The susceptibility satisfies

$$\chi_V(\omega) = \int_{V_{\text{lb}}}^{V_{\text{th}}} v P_1(v)dv = \widehat{P}_1'(0). \quad \text{(B3)}$$

Taking the Laplace transform on either side of Eq. (B2) gives

$$s\widehat{P}_1 = \frac{1}{D}\left(\frac{1}{\tau_m}\frac{\partial \widehat{P}_1}{\partial s} - \mu_0 \widehat{P}_1 + \widehat{J}_1 - \widehat{P}_0\right)$$

$$s\widehat{J}_1 = i\omega\widehat{P}_1 + \chi_s(\omega)(e^{V_{\text{th}}s} - e^{V_{\text{re}}s}),$$

which can be solved to obtain

$$\frac{1}{\tau_m}\frac{\partial \widehat{P}_1}{\partial s} = \left(\mu_0 + sD - \frac{i\omega}{s}\right)\widehat{P}_1$$
$$- \frac{1}{s}(e^{sV_{\text{th}}} - e^{sV_{\text{re}}})\chi_s(\omega) + \widehat{P}_0.$$

Taking the limit as $s \to 0$ on both sides of this equation and using Eq. (B3) yields the expression for $\chi_V(\omega)$ given in Eq. (13)

Since r_s and $\chi_s(\omega)$ are known in closed form Refs. [7,25], the expressions derived above effectively give $\chi_V(\omega)$ in closed form. In addition, the expressions link the statistics of the membrane potentials to the statistics of the output spike trains.

APPENDIX C: A SPIKING EIF MODEL

We now describe the spiking EIF model used for the simulations in Fig. 6. The subthreshold membrane potentials obey [23,38]

$$\frac{dV_k}{dt} = \frac{E_0 - V_k}{\tau_m} + \Delta_T e^{(V_k - V_T)/\Delta_T} + J_e e_k(t) - J_i i_k(t), \quad \text{(C1)}$$

where $e_k(t)$ and $i_k(t)$ are defined as in the methods above. Each time the membrane potential reaches threshold at V_{th}, it is held there for a period of time τ_{spike}, simulating a spike, and is then reset to V_{re}. Active currents are activated when the membrane potential approaches V_T and pull the membrane potential toward V_{th}.

The parameters for Fig. 6 are $\tau_m = 20$ ms, $E_0 = -60$ mV, $V_T = -53$ mV, $\Delta_T = 4$ mV, $V_{\text{th}} = 40$ mV, $V_{\text{re}} = -70$ mV, and $\tau_{\text{spike}} = 1.5$ ms. Note that the absolute refractory period only lasts for 1.5 ms, but a relative refractory period is introduced by the fact that $V_{\text{re}} < E_0$.

APPENDIX D: NUMERICAL METHODS AND SIMULATIONS

Spiking statistics for the LIF were calculated using the threshold integration methods from Ref. [23]. Membrane potential statistics for the LIF were calculated from spiking statistics using the equations derived in Appendix B. All threshold integration calculations use a mesh size of $\Delta v = 0.0005$ when $V_{\text{th}} = 1$ and $V_{\text{re}} = 0$. A lower bound of $V_{\text{lb}} = -3$ was chosen to have an insignificant impact on the statistics calculated. Cross covariances and cross correlations were obtained by taking the inverse Fourier transform on either side of Eqs. (15) and (16). Spike count correlations were obtained from autocovariances and cross covariances using the identities [6,10,11,37]

$$\rho_s(T) = \frac{\int_{-T}^{T}(T - |t|)C_s(t)dt}{\int_{-T}^{T}(T - |t|)A_s(t)dt} \quad \text{and} \quad \lim_{T \to \infty}\rho_s(T) = \frac{\widetilde{C}_s(0)}{\widetilde{A}_s(0)}.$$

Monte Carlo simulations for Figs. 3 and 6 were run for 500 s and 500 trials. Correlated Poisson inputs were generated using the a thinning and jittering algorithm described in Refs. [9,16] and Eqs. (1) and (C1) were each integrated numerically using a first-order Euler method with time bin $\Delta t = 0.05$ ms.

C and MATLAB codes for all figures are available from the first author upon request.

[1] E. Stern, D. Jaeger, and C. Wilson, Nature (London) **394**, 475 (1998).

[2] I. Lampl, I. Reichova, and D. Ferster, Neuron **22**, 361 (1999).

[3] M. Okun and I. Lampl, Nature Neurosci. **11**, 535 (2008).

[4] J. Ziburkus, J. Cressman, E. Barreto, and S. Schiff, J. Neurophysiol. **95**, 01378 (2006).

[5] J. Dorn and D. Ringach, J. Neurophysiol. **89**, 2271 (2003).

[6] T. Tetzlaff, S. Rotter, E. Stark, M. Abeles, A. Aertsen, and M. Diesmann, Neural Comput. **20**, 2133 (2008).

[7] B. Lindner, Ph.D. thesis, Humboldt University, 2002.

[8] A. Yaglom, *An Introduction to the Theory of Stationary Random Functions* (Dover, New York, 2004).

[9] R. Rosenbaum and K. Josić, Neural Comput. **23**, 1261 (2011).

[10] J. de la Rocha, B. Doiron, E. Shea-Brown, K. Josić, and A. Reyes, Nature (London) **448**, 802 (2007).

[11] E. Shea-Brown, K. Josić, J. de la Rocha, and B. Doiron, Phys. Rev. Lett. **100**, 108102 (2008).

[12] R. Rosenbaum, J. Ma, F. Marpeau, A. Barua, and K. Josić, J. Math. Biol., 1 (2011).

[13] H. Tuckwell, *Introduction to Theoretical Neurobiology: Linear Cable Theory and Dendritic Structure*, Vol. 1 (Cambridge University Press, Cambridge, England, 1988).

[14] M. Helias, M. Deger, S. Rotter, and M. Diesmann, Front Neurosci. **5**, 19 (2011).

[15] R. D. Vilela and B. Lindner, Phys. Rev. E **80**, 31909 (2009).

[16] N. Bäuerle and R. Grübel, Astin Bulletin **35**, 379 (2005).

[17] D. Johnson, e-print arXiv:0811.3713.

[18] L. Ricciardi and C. Smith, *Diffusion Processes and Related Topics in Biology* (Springer, New York, 1977).

[19] M. J. E. Richardson and R. Swarbrick, Phys. Rev. Lett. **105**, 178102 (2010).

[20] M. Helias, M. Deger, S. Rotter, and M. Diesmann, PLoS Comput. Biol. **6**, e1000929 (2010).

[21] A. Siegert, Phys. Rev. **81**, 617 (1951).

[22] A. Burkitt, Biol. Cybern. **95**, 1 (2006).

[23] M. J. E. Richardson, Phys. Rev. E **76**, 021919 (2007).

[24] M. Richardson, Biol. Cybern. **99**, 381 (2008).

[25] N. Brunel, F. S. Chance, N. Fourcaud, and L. F. Abbott, Phys. Rev. Lett. **86**, 2186 (2001).

[26] H. Risken, *The Fokker-Planck Equation: Methods of Solution and Applications*, Vol. 18 (Springer Verlag, Berlin, 1996).

[27] S. Ostojic, N. Brunel, and V. Hakim, J. Neurosci. **29**, 10234 (2009).

[28] B. Lindner, B. Doiron, and A. Longtin, Phys. Rev. E **72**, 61919 (2005).

[29] W. Wei and F. Wolf, Phys. Rev. Lett. **106**, 088102 (2011).

[30] P. Bedenbaugh and G. Gerstein, Neural Comput. **9**, 1265 (1997).

[31] E. Stark, A. Globerson, I. Asher, and M. Abeles, J. Neurosci. **28**, 10618 (2008).

[32] H. Super and P. Roelfsema, in *Progress in Brain Research: Development, Dynamics and Pathology of Neuronal Networks*, edited by J. van Pelt, M. Kamermans, C. N. Levelt, A. van Ooyen, G. J. A. Ramakers, and P. R. Roelfsema (Elsevier, New York, 2004), p. 263.

[33] Y. Chen, W. Geisler, and E. Seidemann, Nat. Neurosci. **9**, 1412 (2006).

[34] R. Rosenbaum, J. Trousdale, and K. Josić, Front Neurosci. **5**, 58 (2011).

[35] R. Rosenbaum, J. Trousdale, and K. Josić, Front Comput. Neurosci. **4**, 9 (2010).

[36] A. Rauch, G. La Camera, H. Lüscher, W. Senn, and S. Fusi, J. Neurophysiol. **90**, 1598 (2003).

[37] D. Cox and V. Isham, *Point Processes* (Chapman and Hall/CRC, London, 1980).

[38] N. Fourcaud-Trocmé, D. Hansel, C. Van Vreeswijk, and N. Brunel, J. Neurosci. **23**, 11628 (2003).